https://doi.org/10.5194/egusphere-2026-1501
Preprint. Discussion started: 10 June 2026

Traceable calibration of in-situ aerosol absorption instruments with monodisperse nigrosin

Luka Drinovec[1,2], Jesus Yus-Diez[1,2], Tobias Bühlmann[3], Maitane Iturrate-Garcia[3], Tobias Hammer[4], Konstantina Vasilatou[4], Arun Babu Suja[5], Thomas Müller[5], Krzysztof Ciupek[6], Alejandro Keller[7], Ernest Weingartner[7], Jorge Saturno[8], Maria I. Gini[9], Kostas Eleftheriadis[9], John Backman[10], Eija Asmi[10], Griša Močnik[1,2,11]

[1]Center for Atmospheric Research, University of Nova Gorica, Nova Gorica, 5270, Slovenia
[2]Haze Instruments d.o.o., Ljubljana, 1000, Slovenia
[3]Laboratory Gas Analysis, METAS, Federal Institute of Metrology METAS, Bern, 3003, Switzerland
[4]Particles and Aerosols Laboratory, Federal Institute of Metrology METAS, Bern, 3003, Switzerland
[5]Atmospheric Microphysics Department, Leibniz Institute for Tropospheric Research, 04318 Leipzig, Germany
[6]Air Quality and Aerosol Metrology Group, National Physical Laboratory, Teddington, TW11 0LW, UK
[7]University of Applied Sciences and Arts Northwestern Switzerland, CH-5210 Windisch, Switzerland
[8]Physikalisch-Technische Bundesanstalt, 38116 Braunschweig, Germany
[9]Institute of Nuclear Technology and Radiation, NCSR Demokritos, Paraskevi, Attiki, 15310, Greece
[10]Finnish Meteorological Institute, 00560 Helsinki, Finland
[11]Department of Environmental Sciences, Jozef Stefan Institute, Ljubljana, 1000, Slovenia

Correspondence to: Luka Drinovec (luka.drinovec@ung.si)

Abstract. The absorption coefficient of light absorbing aerosols is difficult to measure with low uncertainty and improvements of measurement procedures based on traceable calibration are needed. Reducing measurement artefacts can be achieved by using in-situ direct measurement methods such as photo-acoustic spectroscopy and photo-thermal interferometry. We developed a traceable calibration method based on monodisperse nigrosin particles. Nebulized nigrosin forms nearly spherical particles for which it is possible to calculate the absorption coefficient in the UV-NIR range using Mie theory. In the presented study, we have experimentally tested size- and mass-selection techniques using a differential mobility analyzer (DMA), a centrifugal particle mass analyzer (CPMA) and a tandem of both in series to compare Mie-calculated absorption coefficient with the measured one using the photo-thermal aerosol absorption monitor PTAAM, traceably calibrated with NO_2. We observed that the nigrosin particle density changes with particle size. Because the absorption coefficient depends mainly on particle mass it is preferrable to base the Mie calculation on the measured particle mass instead of the mobility diameter. Calculated versus measured absorption coefficients differed by +5% to +11% for the DMA, -2% to -3% for the CPMA and +2% to +8% for tandem of the CPMA and the DMA. Combined standard uncertainties (coverage factor k=1) for PTAAM calibrated with monodisperse nigrosin particles selected by the DMA, the CPMA, and the CPMA and the DMA tandem are 6.9%, 5.8% and 5.2%, respectively. The optimal classification setup is a tandem of the CPMA and the DMA which avoids the systematic bias of both neutral (in the CPMA) and multiply-charged (in the DMA) particles and provides a high enough absorption signal. Experimentally the simplest selection method is based on the CPMA.

https://doi.org/10.5194/egusphere-2026-1501
Preprint. Discussion started: 10 June 2026

List of Abbreviations

PTAAM	Photo-thermal aerosol absorption monitor
PTI	Photo-thermal interferometry
PAS	Photo-acoustic spectroscopy
TMPG	Traceable mobile permeation generator
IR	Infrared
UV	Ultraviolet
DMA	Differential mobility analyzer
D_p	Electrical mobility diameter
CPMA	Centrifugal particle mass analyzer
D_m	Mass equivalent diameter
EMS	Extinction minus scattering
CAPS	Cavity attenuated phase shift
FCAE	Faraday cup aerosol electrometer
CPC	Condensation particle counter
b_{abs}	aerosol absorption coefficient

1. Introduction

Absorption and scattering of sunlight by ambient aerosol influence the Earth radiation budget and accurate and precise measurements are required to validate climate models (Bond et al., 2013; Zanatta et al., 2016; Saleh et al., 2018; Samset et al., 2018; Szopa et al., 2021). The aerosol absorption coefficient remains challenging to measure with low uncertainty and improvements in the measurement procedures based on a traceable calibration are needed (Vasilatou et al., 2025). The most common absorption instruments are filter photometers which measure attenuation of light transported through the filter on which particles are continuously collected. These methods suffer from various artefacts caused by the interaction of the particles with the filter matrix, such as cross-sensitivity to scattering (Collaud Coen et al., 2010), filter loading effect (Virkkula et al., 2007; Drinovec et al., 2015), multiple scattering within the filter (Weingartner et al., 2003), and size dependent response (Moteki et al., 2010; Yus-Diez et al., 2021; Romshoo et al, 2022; Drinovec et al., 2022; Yus- Díez et al., 2025). Such artefacts can bias derived intensive properties (eg., single scattering albedo) and aerosol absorption optical depth, propagating into uncertainties in aerosol direct radiative forcing.

Reducing measurement artefacts is possible by using methods which are in-situ and direct, such as photo-acoustic spectroscopy (PAS; Arnott et al., 1999) and photo-thermal interferometry (PTI; Sedlacek, 2006; Drinovec et al., 2022). Measurement methods require calibration, which is usually performed with absorbing gases. The most common absorbing gas used for calibration of PAS is NO_2, which absorbs strongly in the lower half of the visible wavelength range (Arnott et al., 2000; Schnaiter et al. 2023). However, NO_2 absorption in the near-IR region is too low to allow calibration with sub-ppm concentrations. The main drawback with NO_2 for calibration is reaction with the surface material, which reduces sample concentration in tubes and containers (Flores et al., 2021) and complicates the realization of stable, traceable reference concentrations.

Ozone has also been used for calibration of photo-acoustic instruments; however, problems with photo-dissociation and interaction with N_2 have been reported (Bluvshtein et al., 2017; Davies et al., 2018; Fischer and Smith, 2018). Recently, Corbin et al. (2025) proposed a calibration with O_2 at 760 nm, enabling calibration with ambient air. The method is limited to a single wavelength.

https://doi.org/10.5194/egusphere-2026-1501
Preprint. Discussion started: 10 June 2026

An alternative calibration procedure is based on absorbing particles. For spherical particles with known size distribution and refractive index it is possible to calculate the absorption coefficient using Mie theory (Mie, 1908). A popular calibration material is a water-soluble version of nigrosin which can be nebulized to generate polydisperse spherical particles that absorb over a wide spectral range from the UV to the near-IR. The refractive index of the nigrosin sample must be predetermined, for example by using spectroscopy on thin films (Bluvshtein et al., 2017; Drinovec et al., 2022). Care should be taken due to differences in optical properties between batches of nigrosin (Foster et al., 2019). Foster et al. (2019) observed a good agreement between calculated and measured absorption of polydisperse nigrosin. Drinovec et al. (2022) used polydisperse nigrosin to transfer the calibration from the "green" (532 nm) to the IR channel (1064 nm).

Calibration uncertainty can be further reduced by using monodisperse nigrosin particles (Radney and Zangmeister, 2015). To this end, the particle size has been selected using either an aerodynamic aerosol classifier (AAC) (Lawson et al., 2025) or a differential mobility analyzer (DMA) (Lack et al., 2006; Bluvshtein et al., 2017; Cotterell et al., 2020; Kuula et al., 2025).

Here we develop and evaluate a traceable calibration method for aerosol absorption instruments based on monodisperse nigrosin particles. In this study, we experimentally tested size- and mass- selection techniques using a DMA, a centrifugal particle mass analyzer (CPMA) and a tandem configuration of both in series. The DMA provides electrical mobility selection, whereas the CPMA enables mass selection; their tandem use constrains both size and mass simultaneously, improving control over particle properties used for calibration. We assess the performance of these approaches and discuss implications for reducing calibration uncertainty and improving intercomparability across absorption measurement techniques.

2. Materials and methods

2.1 Chemicals

Nigrosin (Acid black 2, Nigrosin water soluble, CAS 8005-03-6) and ammonium sulfate (Mascagnite, ReagentPlus®, CAS 7783-20-2) were obtained from Sigma-Aldrich. Aqueous solutions of nigrosin and ammonium sulfate were prepared by dissolving chemicals in ultra-pure water (Milli-Q). Nigrosin solutions labeled Nig2 (0.1 g L^{-1}) and Nig3 (1 g L^{-1}) have been used for nebulization.

Polystyrene beads (Sigma-Aldrich 433025ML-F) with a particle diameter of 95 nm ± 4% and a density of 1.05 g cm^{-3} were used to validate particle size and mass measurements.

A bottle with a nominal amount fraction of 1 µmol mol^{-1} NO_2 in synthetic air (Traceline, Messer Schweiz AG) was acquired for the PTAAM calibration. For calibration a Tedlar® SCV gas sampling bag (Sigma-Aldrich) was filled with 10 L of sample from the bottle.

2.2 Aerosol absorption measurements

The absorption coefficient was measured using the version P02 of the PTAAM. The PTAAM P02 is based on version P01 described in Drinovec et al. (2022). Instruments differ in the pump lasers used for thermal excitation, with laser diodes (450 nm and 808 nm) being used in P02 instead of diode-pumped solid-state lasers (532 nm and 1064 nm).

The instrument was calibrated following the procedure described by Drinovec et al. (2022). In short, the 450 nm channel was calibrated using a premixed sample of about 1 µmol mol^{-1} NO_2 in synthetic air from the Tedlar bag filled with bottle sample. The exact amount fraction of the premixed sample was measured using a NO_2 cavity attenuated phase shift analyzer (CAPS, Aerodyne Research Inc., USA), which was calibrated using the so-called traceable mobile permeation generator (TMPG, Haerri et al., 2017). NO_2 absorption was calculated based on the spectrum at 450 nm (pump beam) measured with a CCS100/M spectrometer (Thorlabs, USA) and the NO_2 absorption spectrum from Vandaele et al. (2002).

https://doi.org/10.5194/egusphere-2026-1501
Preprint. Discussion started: 10 June 2026

The 808 nm channel was calibrated using polydisperse nigrosin particles transferring the calibration from the blue channel (450 nm) using the Mie calculated $b_{abs\_808\ nm}/b_{abs\_450\ nm}$ ratio. Absorption measurements with the PTAAM were corrected for losses, 2% for NO_2 and 5% for particles (Supplement S7).

The PTAAM was running with 2-minute intervals containing 45 s of background absorption measurement, which was then subtracted from the measured total absorption. Typical instrument noise under controlled laboratory conditions (using filtered room air) is shown in Fig. 1 with 15 min average noise of 0.03 Mm^{-1}. During actual experiments there are influences caused by e.g. pressure oscillations due to several instruments connected to the sample line, or by a possibility of larger variation in room temperature. Actual measurement uncertainty for 15 min experiments of 0.3 Mm^{-1} was determined by the variation of the absorption coefficient for the filtered sample.

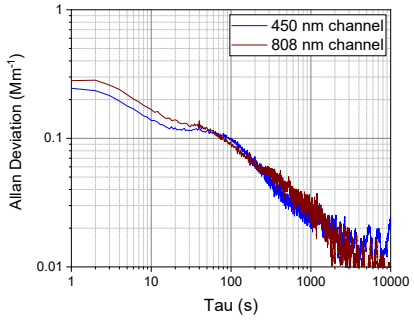

Figure 1. Allan deviation plot for absorption coefficient measured using filtered room air under stable laboratory conditions measured with PTAAM version P02.

2.3 Aerosol generation and classification

Nigrosin and ammonium sulfate aerosols were generated using the ATM 226 nebulizer (Topas GmbH, Germany) at sample flow of 3 L min^{-1} sample flow. The nebulizer was connected to a diffusion drier to reduce relative humidity below 30%.

Particle mass was measured/selected using a centrifugal particle mass analyzer (CPMA, model Mk II, Cambustion Ltd.), as described by Olfert and Collings (2005). The distribution width is defined by a resolution parameter $R_m=m_p/FWHM$, where m_p is the selected particle mass and FWHM is full width at half maximum of the distribution. The CPMA was operated with positive polarity.

Particle mobility diameter was measured/selected using a Vienna-type differential mobility analyzer (DMA, model 2083; TSI Inc., USA). The DMA was operated with negative polarity.

A neutralizer with a Kr-85 source (model 3077A, TSI Inc., USA) was installed upstream of the CPMA and DMA to obtain the Boltzmann charge distribution in the aerosol sample. Particle charge was measured with Faraday-cup aerosol electrometer (FCAE, model 3068B from TSI Inc, USA). Particle number was measured with a condensation particle counter (CPC, model 3750; TSI Inc., USA).

2.4 Data evaluation

All aerosol concentrations were recalculated and reported at conditions of temperature and pressure of 25 °C and 100 kPa.

https://doi.org/10.5194/egusphere-2026-1501
Preprint. Discussion started: 10 June 2026

Mie calculations were performed using MATLAB routines for homogeneous spheres (Mätzler, 2002). The refractive index of the Nigrosin batch was used in this study had been determined previously and was taken as 1.58 + i0.167 at 450 nm and 1.78 + i0.119 at 808 nm (Drinovec et al., 2022b) for the calculation of absorption coefficients.

Measurement noise (standard error) was 0.1-0.2% for the CPC, 0.5-1.5% for the FCAE and 0.3-0.5% for the PTAAM. A typical experiment time series is shown in Supplement (Fig. S1).

3. Results

3.1 Density of nigrosin particles

Particle density was measured for monodisperse particles whose mass m_p was selected by the CPMA and mobility diameter D_p measured by the SMPS as shown in Fig. 2. The CPMA was run at R_m=10 which resulted in distribution width of 10% of their selected mass. The number size distributions (Fig. 3A) show two peaks corresponding to the mobility diameter of the doubly- and singly-charged particles. The distributions were fitted with two Gauss functions to obtain the peak mobility diameter. Effective particle density and particle volume were calculated based on the selected particle mass (Fig. 3A) and the mobility diameter, respectively. For nigrosin, the effective density increases with particle mass toward the nominal value of 1.6 g cm^{-3} (Moteki et al., 2010). Similar behavior was observed for the nebulized ammonium sulfate (Supplement - Fig. S2) but not for the 95 nm polystyrene beads, where the measured density agreed with the nominal value within 0.8% (Supplement – Table S1). The low experimental values in the particle density for nigrosin might be due to fusion of particles before being completely dry. Fused particles were found on nigrosin filter samples analyzed by SEM (Supplement – Fig. S5)

Because the absorption coefficient depends mainly on particle mass, we decided to use the mass-equivalent particle diameter D_m for Mie calculations, which is smaller than D_p for all the measured sizes (Table 1). The absorption coefficients calculated based on the measured mobility diameter results in 5-20% higher values compared to calculations based on D_m.

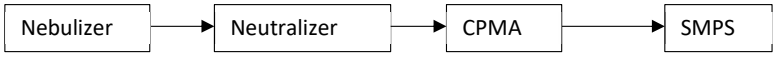

Figure 2. Schematic diagram of the experimental setup for particle density measurement.

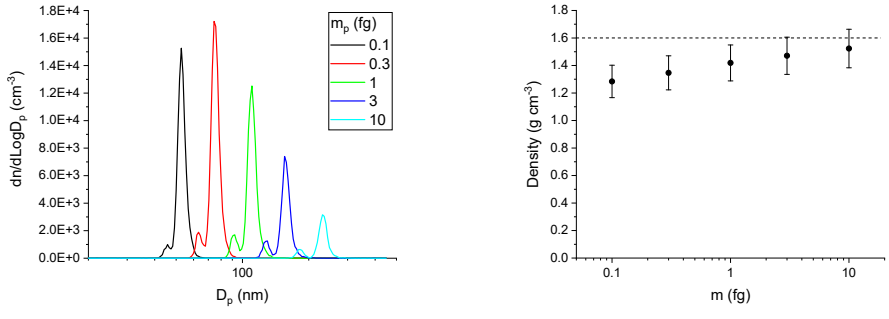

(A) (B)

Figure 3. Electrical mobility number size distributions for nigrosin particles at different target masses (A), shown without correction for multiple charge. Nigrosin particle density (B) as a function of particle mass. Error bars represent measurement uncertainty of 9% (coverage factor_*k*= 1; 68% confidence interval). The dashed line represents a density of 1.6 g cm^{-3}, as reported by Moteki et al. (2010).

https://doi.org/10.5194/egusphere-2026-1501
Preprint. Discussion started: 10 June 2026

Table 1. Measured mobility diameter D_p, effective density and mass-equivalent diameter D_m for nigrosin particles selected according to particle mass (m_p). Uncertainties (k=1) for particle mass, mobility dimeter, effective density and mass equivalent diameter are 2%, 3%, 9.2% and 0.7%, respectively.

m_p (fg)	D_p (nm)	Effective density (g cm^{-3})	D_m (nm) for ρ=1.6 g cm^{-3}
0.1	53.0	1.28	49.2
0.3	75.2	1.35	71.0
1	110.4	1.42	106.1
3	157.4	1.47	153.0
10	232.3	1.52	228.5

3.2 Absorption of polydisperse nigrosin particles

For a polydisperse distributions, the absorption coefficients calculated for each size bin were summed. These depend on the correct charge inversion algorithm which predicts the total particle number concentration from that obtained for singly-charged particles corrected for multiply-charged particles and diffusion losses. The calculated number and volume size distribution are shown in Fig 4A.

The volume size distribution shows the presence of particles above 350 nm, which represent a non-negligible fraction of total volume. Experiments with an impactor (not shown) failed to reduce the number of these particles, indicating an artefact related to limitations of the inversion algorithm. For the Mie calculation of the sample absorption, only particles smaller than 400 nm were used.

Because of the nigrosin density size dependence (Fig. 3B), a size distribution based on the mass equivalent diameter D_m was used for the Mie calculation. The calculated absorption coefficient was 10% larger than the measured one at 450 nm (Fig. 4B). Because of the charge inversion, the uncertainty of particle number concentration for the polydisperse size distribution is 10% (Wiedensohler et al., 2018) which strongly influences the combined uncertainty for the calibration with polydisperse nigrosin (Table 2).

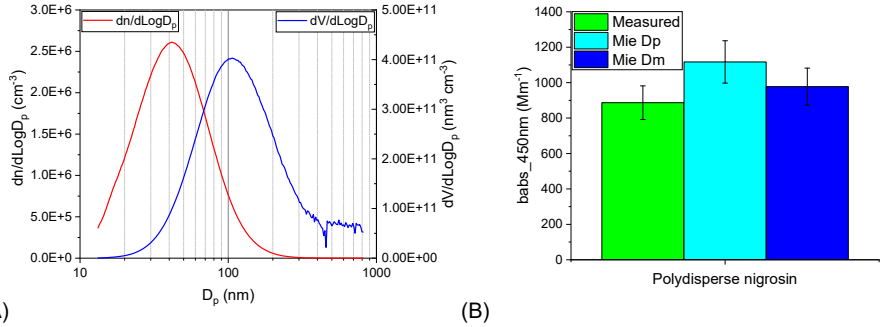

(A) (B)

Figure 4. Measured particle size distributions of nigrosine aerosols (solution Nig2) shown as number-based and volume-based distributions as a function of mobility diameter (A). Comparison between measured absorption coefficient and the absorption coefficient calculated using Mie theory based on the particle mobility diameter D_p and mass-equivalent diameter D_m (B).

https://doi.org/10.5194/egusphere-2026-1501
Preprint. Discussion started: 10 June 2026

3.3 Monodisperse nigrosin particles selected with a differential mobility analyzer (DMA)

The first particle selection approach investigated in this study is based on size selection, performed using electrical mobility classification with a DMA. For each selected mobility diameter, the particle number concentration and absorption coefficient were measured using a CPC and a PTAAM, respectively (Fig. 5). DMA-based size selection is likely to remain the most common. However, electrical mobility selection intrinsically includes both singly charged particles at the target diameter and larger multiply charged particles with the same mobility, which must be considered when interpreting size-resolved number, mass, and absorption measurements. To reduce the fraction of multiply-charged particles (and the corresponding error), we shifted the selection to the descending side of the volume size distribution. This was achieved by nebulizing a more diluted nigrosin solution (Figure 6A).

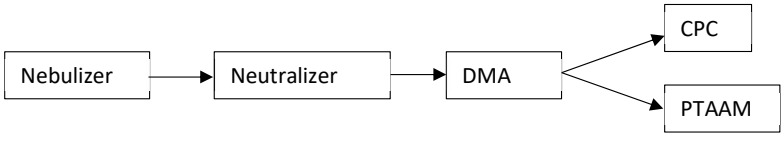

Figure 5. Schematic diagram of the experimental setup for particle size selection by differential mobility analyzer (DMA).

We quantified the bias due to the multiply-charged particles, transmitted by the DMA, on the measured absorption coefficient. The number of multiply-charged particles was determined by measuring the particle mass distribution using a CPMA followed by a CPC downstream of the DMA, essentially inserting the CPMA between the DMA and CPC in Fig. 5. The numbers of singly-, doubly- and triply-charged particles were calculated by fitting Gauss functions to the measured distribution and integrating each peak (Supplement – Fig. S4). The absorption was then calculated as the sum of the absorption of singly-charged particles with mass m_0, doubly-charged particles with mass $3.5*m_0$ and triply-charged particles with mass $6.6*m_0$. In our experiment, multiply-charged particles accounted for 15% and 25% of the total light absorption.

To obtain sufficient signal when using a more diluted nigrosin solution for nebulization a relatively broad mass distribution ($R_m=m_p$/FWHM=1.5) is used. This was achieved by sample-to-sheet flow ratio of 1.5 L min^{-1}/5 L min^{-1}. For the selected particle distributions, we measured an absorption coefficient of approx. 20 Mm^{-1} (Figure 6B). The comparison between the measured and calculated absorption coefficients for three different particle sizes was based on the measured particle mass for each setting (Figure 6B). The calculated absorption after correction for multiply charged particles was higher than the measured one by 5%, 11% and 7% for particles with mass 0.7, 2.4, and 5.7 fg, respectively.

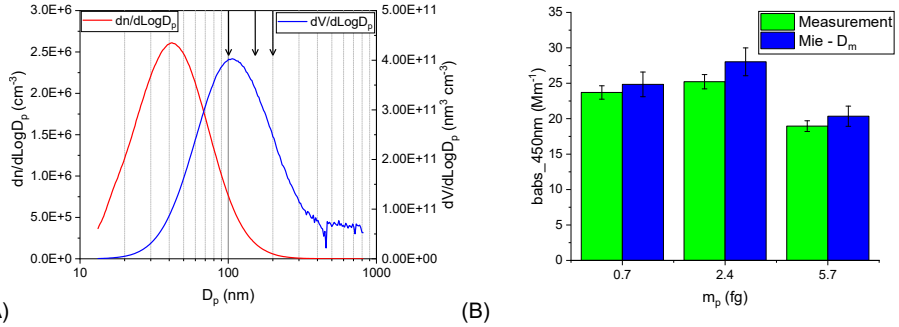

Figure 6. Measured particle size distributions of nigrosin aerosols, generated by nebulizing nigrosin solution Nig2 (0.1 g L^{-1}), shown as number based and volume-based distributions as a function of mobility diameter. Arrows show the selected mobility diameters (A). Comparison between the measured absorption coefficient and the calculated absorption coefficient based on the mass-equivalent diameter D_m (B).

https://doi.org/10.5194/egusphere-2026-1501
Preprint. Discussion started: 10 June 2026

3.4 Monodisperse nigrosin particles selected with a centrifugal particle mass analyzer (CPMA)

The particles were selected with a CPMA and their charge is measured with a FCAE, as shown in Fig. 7. Similar to the DMA, the CPMA transmits multiply-charged particles. In this experimental setup, however, the mass of the charged particles is directly proportional to their charge, so that the measured current closely corresponds to the particle mass concentration. The absorption coefficient of two particles with the selected mass differs from one particle with double mass because the mass absorption cross-section slowly increases with size (Supplement Fig. S3), at the selected mass of 1 fg the difference is 2%. Because the fraction of the multiply charged particles is several times smaller compared to the singly charged particles the error is smaller than 1% and the correction was not applied.

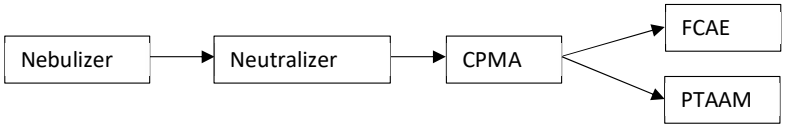

Figure 7. Schematic diagram of the experimental setup for particle mass selection using a centrifugal particle mass analyzer (CPMA).

The width of the mass distribution of the CPMA-selected particles depends on the resolution parameter R_m. At low R_m, we obtain higher particle number and absorption, together with neutral particles that leak through the classifier. These neutral particles are expected to have low mass, but their exact number and corresponding absorption is difficult to predict (Johnson et al., 2013). The relative number of neutral particles can be reduced by selecting the particles on the ascending part of the particle volume distribution. This was achieved by nebulizing a more concentrated nigrosin solution (Figure 10A).

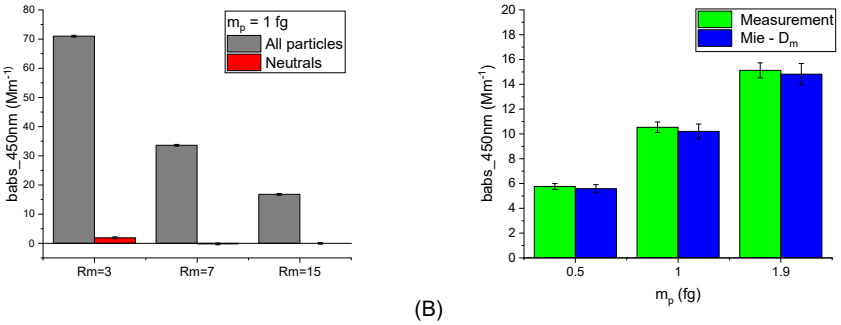

Figure 8. The absorption coefficient of total and neutral-only particles transmitted through the CPMA for different values of the resolution parameter R_m(A). Comparison between measured absorption coefficient and the absorption coefficient calculated, based on mass-equivalent diameter D_m, for different particle masses selected by means of a CPMA with Rm=15 (B).

Neutral particles were analyzed by running the sample through an electrostatic precipitator (DMA set to a voltage of -10000 V without the sheath flow). When running the CPMA at R_m=3, neutral particles represent 2.6% of the total absorption (Fig. 8A). At higher R_m values, the absorption due to neutral particles is negligible. A final comparison between measured and calculated absorption was performed for R_m=15 (Fig. 8B). There is a good agreement between the measured and calculated absorption which is lower by 2-3%. As discussed above, the R_m=7 setting would be sufficient to eliminate neutral particles and would double the absorption signal.

https://doi.org/10.5194/egusphere-2026-1501
Preprint. Discussion started: 10 June 2026

3.5 Monodisperse nigrosin particles selected with the tandem CPMA and DMA setup

In the tandem setup, particles are first selected by mass using the CPMA and then filtered by setting the DMA to the peak mobility diameter for the selected mass point. For example, we set the CPMA to select 1 fg particles, then the DMA should be set to mobility diameter of 110.4 nm for nigrosin particles. The main advantage of this setup is the elimination of neutral and multiply-charged particles. Neutral particles are filtered out by the DMA. Multiply-charged particles are likewise not transmitted because the CPMA and DMA behave differently: in the CPMA multiply-charged particles have multiple masses ($2*m_0$, $3*m_0$, ...) but in the DMA these particles appear at their multiple mobilities (for m_0=1 fg we obtain a mobility diameter of 93 nm and 80 nm for doubly- and triply- charged particles).

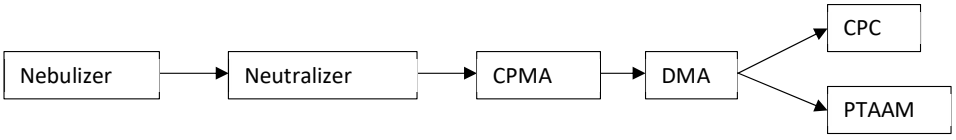

Figure 9. Schematic diagram of the experimental setup for particle size selection using a tandem of centrifugal particle mass analyzer (CPMA) and differential mobility analyzer (DMA).

Because the neutral particles are removed, it is possible to set CPMA to lower resolution R_m and to obtain higher absorption signal. We run the classifiers CPMA with R_m=5 and DMA with R_m=3. Without neutral and multiply charged particles it was possible to measure the particle concentration using CPC instead of FCAE with the advantage of lower measurement noise. The results show that the calculated absorption is higher than the measured one by 8%, 5% and 2% for 1 fg, 3 fg and 10 fg particles, respectively (Fig. 10B).

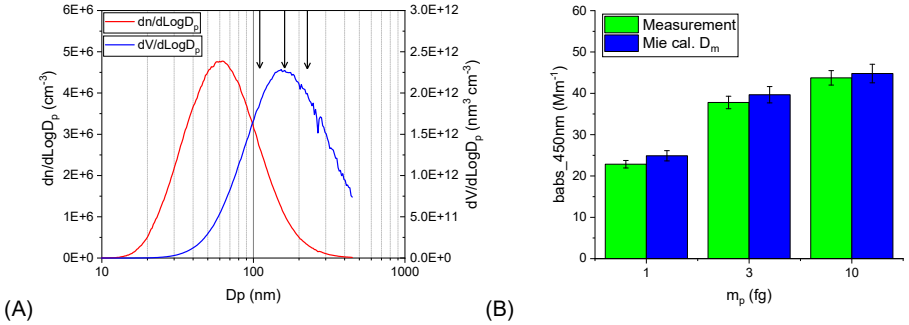

Figure 10. Measured particle size distributions of nigrosin aerosols, generated by nebulizing nigrosin solution Nig3 (1 g L^{-1}), shown as number based and volume-based distributions as a function of mobility diameter. Arrows show the selected mobility diameters (A). Comparison between measured and calculated absorption coefficient based on mass-equivalent diameter D_m (B).

https://doi.org/10.5194/egusphere-2026-1501
Preprint. Discussion started: 10 June 2026

3.6 Uncertainty analysis of the PTAAM (version P02) for different calibration schemes

The uncertainty in the absorption coefficient measured with the PTAAM results from calibration method and instrumental uncertainties (Table 2). The combined uncertainty is calculated as the square-root of the linear sum of squared standard uncertainty components for a coverage factor k=1 (68 % confidence interval).

The calibration of the 450 nm channel depends strongly on the uncertainty in the NO_2 amount fraction in the calibrating gas mixture. For NO_2 mixtures produced by the TMPG, the standard uncertainty of the NO_2 amount fraction is below 2% (Haerri et al., 2017). The uncertainty budget from Drinovec et al. (2022) is updated here with the uncertainty of the NO_2 absorption spectrum (Vandaele et al., 2002; Orphal and Chance, 2003). For nigrosin particles, the uncertainties in the real and imaginary part of the refractive index (2% and 3%, respectively) result in a 2% uncertainty of the calculated absorption coefficient. The uncertainty in the measured number size distribution by the SMPS, which affects the calculation of polydisperse nigrosin absorption, is 10% (Wiedensohler et al., 2018). The influence of the size distribution on the absorption ratio b_{abs}(808 nm)/b_{abs}(450 nm) is lower, having 4% uncertainty. When monodisperse nigrosin is produced with DMA, the calculated absorption coefficient must take into account the multiply charged particles which account for 15-25% of absorption. We accessed 5% additional uncertainty in the calculated absorption coefficient caused by errors in multiple-charge correction.

Table 2. Sources of uncertainty and combined standard uncertainties (for 68% and 95% confidence intervals CI) of the absorption coefficient of PTAAM, which was traceably calibrated with gas and particles. Combined uncertainties were calculated using independent uncertainty components.

Source of uncertainty		**Uncertainty k=1 (68% CI)**	**Uncertainty k=2 (95% CI)**
A: NO_2 amount fraction		2%	
B: Absorption cross-section of NO_2		2%	
C: Mie calculation & nigrosin refractive index		2%	
D: Influence of particle size distribution error on absorption ratio babs(808 nm)/babs(450 nm)		4%	
E: Particle number size distribution measured by SMPS		10%	
F: CPC measurement uncertainty		3%	
G: FCAE measurement uncertainty		4%	
H: DMA uncertainty after charge correction		5%	
I: CPMA mass uncertainty		2%	
J: Scattering and absorbing gases		1%	
K: Stability of PTAAM response		3%	
Combined uncertainties	**Contributions**		
PTAAM 450 nm: calibration with NO_2	A, B, J, K	4.2%	8.4%
PTAAM 450 nm: polydisperse nigrosin	C, E, J, K	10.7%	21.4%
PTAAM 808 nm: NO2 + polydisperse nigrosin	A, B, C, D, J, K	6.2%	12.4%
Monodisperse nigrosin – DMA	C, F, H, J, K	6.9%	13.8%
Monodisperse nigrosin – CPMA	C, G, I, J, K	5.8%	11.6%
Monodisperse nigrosin – CPMA + DMA	C, F, I, J, K	5.2%	10.4%

https://doi.org/10.5194/egusphere-2026-1501
Preprint. Discussion started: 10 June 2026

The uncertainty in the particle number concentration measured by the CPC depends on the calibration and flow measurement, resulting in 3% uncertainty (Wiedensohler et al., 2018). Due to high noise at low sample flow, a 4% uncertainty was used for the FCAE. The uncertainty in mass selection by the CPMA is 2% (Titosky et al., 2019).

Instrument operation can be influenced by the scattering artefact (0.1% as reported by Drinovec et al., (2022)) and the presence of absorbing gases; absorption of gas fraction is measured on filtered sample and subtracted from the total absorption, however interactions from the adsorbed gas are also possible. The uncertainty contribution from the stability of the instrument response (3%) was determined by Kalbermatter et al. (2022).

4. Discussion

A combination of DMA and CPMA has been extensively used in the past to measure the effective/material density of aerosols such as soot and organics. For nigrosin, we found that the particle density differed from the 1.6 g cm^{-3} value reported by Moteki et al. (2010), with the difference being higher for smaller particles. Particle density strongly influences modeled absorption when calculated using the measured mobility diameter. To determine the correct particle absorption coefficients, a particle mass (or mass-equivalent diameter) should be used in the Mie calculations. Due to variable particle density, a mass classifier (CPMA) is preferred over a size classifier (DMA). Consequently, the Mie-calculated absorption of polydisperse nigrosin, taking into account the correct density, agrees within 10% with absorption measurements obtained with the PTAAM. The main source of uncertainty in the modeled absorption coefficient of polydisperse nigrosin is the charge correction in the SMPS. The calculated k=1 uncertainties for calibration with monodisperse nigrosin using a DMA, a CPMA or a tandem of the CPMA and the DMA in series are much lower (6.9%, 5.8% and 5.2%, respectively) compared to the calibration with polydisperse nigrosin (10.7%). The lower uncertainty for monodisperse nigrosin leads to lower differences between measured and calculated absorption.

When using a DMA for size selection, we have to correct for multiply-charged particles. To reduce the number of multiply-charged particles, it helps to select particles on the right side of the volume size distribution. This requires nebulizing a more diluted nigrosin solution. To obtain a high enough particle number concentrations, the resolution of the DMA must be decreased, which can reduce the accuracy of the monodisperse aerosol approach. The influence of multiple-charge with a DMA selection can be reduced by the impactor which removes bigger particles (Bluvshtein et al., 2017; Kuula et al., 2025).

When using a CPMA, we have to account for the contribution of neutral particles. Their contribution can be reduced by increasing the concentration of the nebulized nigrosin solution and using a sufficiently high R_m value (Rm>7). Experimentally, calibration using a CPMA and FCAE is the simplest and requires no additional instrumentation. The highest absorption signal can be obtained using a tandem of the CPMA and the DMA for which there is no contribution from neutral and multiply-charged particles, and a medium R_m value can be used for both classifiers. A comparison between different methods is summarized in Table 3.

Particle size selection can also be performed using the AAC, resulting in a much higher absorption signal compared to the CPMA and the DMA, because for the AAC the particles are not filtered by charge (Lawson et al. 2025). A monodisperse particle size distribution can also be produced using a combination of unipolar charger and CPMA (Titosky et al., 2019). Unipolar charger produces a narrow distribution of highly charged particles resulting in a particle mass several times bigger than the CPMA setpoint, with the mass depending on the particle size and morphology (Hassim et al., 2025). For both selection methods an additional classifier is needed to determine the resulting particle mass.

https://doi.org/10.5194/egusphere-2026-1501
Preprint. Discussion started: 10 June 2026

Table 3. A comparison between the absorption calibration methods used in this study, based on polydisperse nigrosin particles and monodisperse nigrosin particles selected using a DMA, a CPMA or a tandem configuration of CPMA and DMA.

	Polydisperse	Monodisperse		
	/	DMA	CPMA	CPMA+DMA
Resolution parameter R_m	0.1	1.5	15	CPMA:5, DMA:3
b_{abs}_450 nm (Mm-1)	887	25.2 (m_p=2.4 fg)	14.5 (m_p=1.9 fg)	38 (m_p=3 fg)
b_{abs} calculated vs. measured	+10%	+5 to +11%	-2% to -3%	+2% to +8%
Postprocessing	Density correction	Multiple charge correction	/	/
Needed instrumentation	DMA, CPMA, CPC	DMA, CPMA, CPC	CPMA, FCAE	DMA, CPMA, CPC
Uncertainty (k=1)	10.7%	6.9%	5.8%	5.2%

5. Conclusions

Measured nigrosin particle density differed by up to 20% from the reference value of 1.6 g cm^{-3}. Because the absorption coefficient depends mainly on particle mass it is preferrable to base the Mie calculation on the measured particle mass instead of the mobility diameter.

Mie calculated absorption coefficient for polydisperse and monodisperse nigrosin particles at 450 nm was compared with measurements using the PTAAM, which was previously calibrated with NO_2. Calibration of the absorption instruments with monodisperse nigrosin (selected with the CPMA or a tandem of the CPMA and the DMA) yields lower measurement uncertainty and better experimental agreement with measurements, compared to a polydisperse or a DMA selected sample.

The DMA selection method suffers from uncertainties due to multiply-charged particles, resulting in higher uncertainty compared to other methods.

The CPMA selection requires a high enough resolution parameter R_m value to avoid the influence of neutral particles. Application of high R_m results in a lower particle number (and corresponding absorption coefficient) available for the calibration.

Configuration with a CPMA and a FCAE is the simplest calibration method because it requires only a CPMA and a FCAE without the need for post processing. The optimal classification setup is a tandem of the CPMA and the DMA in series which avoids the biases caused by neutral and multiply-charged particles and provides high absorption signal and lowest uncertainty.

Acknowledgments

This work was supported by EURAMET (22NRM02 STANBC project), the Slovenian research and innovation agency (P1-0385, I-0033, L2-4485) and ESA (4000131931/20/NL/FF/an). The project 22NRM02 STANBC has received funding from the European Partnership on Metrology, co-financed from the European Union's Horizon Europe Research and Innovation Program and by the Participating States. AI has not been used in any stage of research or article preparation.

Conflict of interest statement

LD, GM and JYD are employed by Haze Instruments d.o.o., the PTAAM manufacturer. GM is an editor for AMT.

https://doi.org/10.5194/egusphere-2026-1501
Preprint. Discussion started: 10 June 2026

Data repository

Data is available at https://repozitorij.ung.si/IzpisGradiva.php?id=11081.

Author contributions

LD performed the experiments, evaluated the data and prepared the manuscript. EA provided and calibrated the FCAE. TB and MIG performed calibration of PTAAM and NO_2 CAPS with TMPG. All coauthors helped with manuscript preparation.

References

Arnott, W. P., Moosmüller, H., Rogers, C. F., Jin, T., and Bruch, R.: Photoacoustic spectrometer for measuring light absorption by aerosol: instrument description, Atmos. Environ., 33, 2845–2852, 1999.

Arnott, W. P., Moosmüller, H., and Walker, J. W.: Nitrogen dioxide and kerosene-flame soot calibration of photoacoustic instruments for measurements of light absorption by aerosols, Rev. Sci. Instr., 71, 4545–4552, https://doi.org/10.1063/1.1322585, 2000.

Bluvshtein, N., Flores, J. M., He, Q., Segre, E., Segev, L., Hong, N., Donohue, A., Hilfiker, J. N., and Rudich, Y.: Calibration of a multi-pass photoacoustic spectrometer cell using light-absorbing aerosols, Atmos. Meas. Tech., 10, 1203–1213, https://doi.org/10.5194/amt-10-1203-2017, 2017.

Bond, T. C., Doherty, S. J., Fahey, D. W., Forster, P. M., Berntsen, T., DeAngelo, B. J., Flanner, M. G., Ghan, S., Karcher, B., Koch, D., Kinne, S., Kondo, Y., Quinn, P. K., Sarofim, M. C., Schultz, M. G., Schulz, M., Venkataraman, C., Zhang, H., Zhang, S., Bellouin, N., Guttikunda, S. K., Hopke, P. K., Jacobson, M. Z., Kaiser, J. W., Klimont, Z., Lohmann, U., Schwarz, J. P., Shindell, D., Storelvmo, T., Warren, S. G., and Zender, C. S.: Bounding the role of black carbon in the climate system: A scientific assessment, J. Geophys. Res.-Atmos., 118, 5380–5552, https://doi.org/10.1002/jgrd.50171, 2013.

Collaud Coen, M., Weingartner, E., Apituley, A., Ceburnis, D., Fierz-Schmidhauser, R., Flentje, H., Henzing, J. S., Jennings, S. G., Moerman, M., Petzold, A., Schmid, O., and Baltensperger, U.: Minimizing light absorption measurement artifacts of the Aethalometer: evaluation of five correction algorithms, Atmos. Meas. Tech., 3, 457–474, https://doi.org/10.5194/amt-3-4572010, 2010.

Corbin, J. C., Moallemi, A., Poitras, D., Sipkens, T. A., & Norooz Oliaee, J.: Self-calibrating aerosol absorption measurements using co-located TDLAS and tunable-wavelength photothermal interferometry. Aerosol Science and Technology, 59(7), 877–891. https://doi.org/10.1080/02786826.2025.2469780, 2025.

Cotterell, M. I., Szpek, K., Haywood, J. M., & Langridge, J. M.: Sensitivity and accuracy of refractive index retrievals from measured extinction and absorption cross sections for mobility-selected internally mixed light absorbing aerosols. Aerosol Science and Technology, 54(9), 1034–1057. https://doi.org/10.1080/02786826.2020.1757034, 2020.

Davies, N. W., Cotterell, M. I., Fox, C., Szpek, K., Haywood, J. M., and Langridge, J. M.: On the accuracy of aerosol photoacoustic spectrometer calibrations using absorption by ozone, Atmos. Meas. Tech., 11, 2313–2324, https://doi.org/10.5194/amt-11-2313-2018, 2018.

Drinovec, L., Močnik, G., Zotter, P., Prévôt, A. S. H., Ruckstuhl, C., Coz, E., Rupakheti, M., Sciare, J., Müller, T., Wiedensohler, A., and Hansen, A. D. A.: The "dual-spot" Aethalometer: an improved measurement of aerosol black carbon with realtime loading compensation, Atmos. Meas. Tech., 8, 1965–1979, https://doi.org/10.5194/amt-8-1965-2015, 2015.

https://doi.org/10.5194/egusphere-2026-1501
Preprint. Discussion started: 10 June 2026

Drinovec, L., Jagodič, U., Pirker, L., Škarabot, M., Kurtjak, M., Vidović, K., Ferrero, L., Visser, B., Röhrbein, J., Weingartner, E., Kalbermatter, D. M., Vasilatou, K., Bühlmann, T., Pascale, C., Müller, T., Wiedensohler, A., and Močnik, G.: A dual-wavelength photothermal aerosol absorption monitor: design, calibration and performance, Atmos. Meas. Tech., 15, 3805–3825, https://doi.org/10.5194/amt-15-3805-2022, 2022.

Drinovec, L., Jagodič, U., Pirker, L., Škarabot, M., Kurtjak, M., Vidović, K., Ferrero, L., Visser, B., Röhrbein, J., Weingartner, E., Kalbermatter, D. M., Vasilatou, K., Bühlmann, T., Pascale, C., Müller, T., Wiedensohler, A., and Močnik, G.: Supplement of: A dual-wavelength photothermal aerosol absorption monitor: design, calibration and performance, Atmos. Meas. Tech., 15, 3805–3825, https://doi.org/10.5194/amt-15-3805-2022-supplement, 2022b.

Fischer, D. A. and Smith, G. D.: Can ozone be used to calibrate aerosol photoacoustic spectrometers? Atmos. Meas. Tech., 11, 6419–6427, https://doi.org/10.5194/amt-11-6419-2018, 2018.

Flores, E., Viallon, J., Idrees, F., Moussay, P., Wielgosz, R., Shinji, U. I., Cieciora, D., Rolle, F., Sega, M., Sang-Hyub, O., Macé, T., Sutour, C., Pascale, C., Zhang, T., Wang, D., Guo, H., Han, Q., Smeulders, D., Jozela, M., Ntsasa, N. G., Tshilongo, J., Mphamo, T., Van Aswegen, S., Worton, D., Brewer, P., Valkova, M., Tarhan, T., Efremova, O., Konopelko, L., de Krom, I., Persijn, S., and van der Veen, A.: Final report on international comparison CCQM-K74: Nitrogen dioxide, 10µmol/mol, Metrologia, 58, 08018, https://doi.org/10.1088/0026-1394/58/1A/08018, 2021.

Foster, K., Pokhrel, R., Burkhart, M., and Murphy, S.: A novel approach to calibrating a photoacoustic absorption spectrometer using polydisperse absorbing aerosol, Atmos. Meas. Tech., 12, 3351–3363, https://doi.org/10.5194/amt-12-3351-2019, 2019.

Haerri, H.-P., Macé, T., Waldén, J., Pascale, C., Niederhauser, B., Wirtz, K., Stovcik, V., Sutour, C., Couette, J., and Waldén, T.: Dilution and permeation standards for the generation of NO, NO2 and SO2 calibration gas mixtures, Meas. Sci. Technol., 28, 035801, https://doi.org/10.1088/1361-6501/aa543d, 2017.

Hassim, J., Risby, K., Reavell, K., & Hochgreb, S.: Multiple charge correction in particle mass analyzers: Experimental validation of the interpolated average charge (INTAC) algorithm. Aerosol Science and Technology, 59(12), 1566–1585. https://doi.org/10.1080/02786826.2025.2523930, 2025.

Johnson, T. J., Symonds, J. P. R. and Olfert, J. S.: Mass–Mobility Measurements Using a Centrifugal Particle Mass Analyzer and Differential Mobility Spectrometer, Aerosol Science and Technology, 47(11), 1215–1225. doi: 10.1080/02786826.2013.830692, 2013.

Kalbermatter, D. M., Mocnik, G., Drinovec, L., Visser, B., Röhrbein, J., Oscity, M., Weingartner, E., Hyvärinen, A.-P., and Vasilatou, K.: Supplement of "Comparing black-carbon- and aerosol-absorption measuring instruments – a new system using lab-generated soot coated with controlled amounts of secondary organic matter", Atmos. Meas. Tech., 15, 561–572, https://doi.org/10.5194/amt-15-561-2022-supplement, 2022.

Kuula, J., Karhu, J., Mikkonen, T., Grahn, P., Virkkula, A., Timonen, H., Hieta, T., and Vainio, M.: Validation of cantilever-enhanced photoacoustic particle-size-resolved light absorption measurement using nigrosin reference particles and Mie modelling, Aerosol Research, 3, 1–13, https://doi.org/10.5194/ar-3-1-2025, 2025.

Lack, D. A., Lovejoy, E. R., Baynard, T., Pettersson, A., and Ravishankara, A. R.: Aerosol absorption measurement using photoacoustic spectroscopy: Sensitivity, calibration, and uncertainty developments, Aerosol Sci. Tech., 40, 697–708, https://doi.org/10.1080/02786820600803917, 2006.

Lawson, G. R., Chen, S. X., Collins, G., Lawson, N., Szpek, K., Bowles, J.,Allan, J., Langridge, J.M. and Cotterell, M. I.: An innovative approach to characterizing the refractive indices and effective densities of internally mixed light-absorbing aerosol particles. Aerosol Science and Technology, 59(7), 857–876. https://doi.org/10.1080/02786826.2025.2468966, 2025.

https://doi.org/10.5194/egusphere-2026-1501
Preprint. Discussion started: 10 June 2026

Mätzler, C.: MATLAB Functions for Mie Scattering and Absorption, Institute of Applied Physics, University of Bern, IAP Research Report No. 2002-08, https://omlc.org/software/mie/maetzlermie/Maetzler2002.pdf (last access: 22 June 2022), 2002.

Mie, G.: Beiträge zur Optik trüber Medien, speziell kolloidaler Metallösungen, Annalen der Physik, 330 (3), 377–445, doi:10.1002/andp.19083300302, 1908.

Moteki, N., Kondo, Y., Nakayama, T., Kita, K., Sahu, L.K., Ishigai, T., Kinase, T. and Matsumi, Y.: Radiative transfer modeling of filter-based measurements of light absorption by particles: Importance of particle size dependent penetration depth, Journal of Aerosol Science, 41 (4), 401-412, https://doi.org/10.1016/j.jaerosci.2010.02.002, 2010.

Olfert, J. S. and Collings, N.: New method for particle mass classification- the Couette centrifugal particle mass analyzer, J. Aerosol Sci., 36, 1338–1352, 2005.

Orphal, J. and Chance, K.: Ultraviolet and visible absorption crosssections for HITRAN, J. Quant. Spectrosc. Ra., 82, 491–504, https://doi.org/10.1016/S0022-4073(03)00173-0, 2003.

Presser, C.: Absorption coefficient measurements of particle-laden filters using laser heating: Validation with nigrosin, J. Quant. Spectrosc. Radiat. Transfer, 113 (8), 607-623, https://doi.org/10.1016/j.jqsrt.2012.01.009, 2012.

Radney, J.G. and Zangmeister, C.D.: Measurement of Gas and Aerosol Phase Absorption Spectra across the Visible and Near-IR Using Supercontinuum Photoacoustic Spectroscopy, Anal. Chem., 87 (14), 7356-7363, doi: https://10.1021/acs.analchem.5b01541, 2015.

Romshoo, B., Pöhlker, M., Wiedensohler, A., Pfeifer, S., Saturno, J., Nowak, A., Ciupek, K., Quincey, P., Vasilatou, K., Ess, M. N., Gini, M., Eleftheriadis, K., Robins, C., Gaie-Levrel, F., and Müller, T.: Supplement of : Importance of size representation and morphology in modelling optical properties of black carbon: comparison between laboratory measurements and model simulations, Atmos. Meas. Tech., 15, 6965–6989, https://doi.org/10.5194/amt-15-6965-2022-supplement, 2022.

Saleh, R., Cheng, Z., and Atwi, K.: The Brown-Black Continuum of Light-Absorbing Combustion Aerosols, Environ. Sci. Tech. Let., 5, 508–513, https://doi.org/10.1021/acs.estlett.8b00305, 2018.

Samset, B. H., Sand, M., Smith, C. J., Bauer, S. E., Forster, P. M., Fuglestvedt, J. S., Osprey, S., and Schleussner, C. F.: Climate Impacts From a Removal of Anthropogenic Aerosol Emissions, Geophys. Res. Lett., 45, 1020–1029, https://doi.org/10.1002/2017GL076079, 2018.

Schnaiter, F. M., Linke, C., Asmi, E., Servomaa, H., Hyvärinen, A.-P., Ohata, S., Kondo, Y., and Järvinen, E.: The four-wavelength Photoacoustic Aerosol Absorption Spectrometer (PAAS-4λ), Atmos. Meas. Tech., 16, 2753–2769, https://doi.org/10.5194/amt-16-2753-2023, 2023.

Sedlacek III, A. J.: Real-time detection of ambient aerosols using photothermal interferometry: Folded Jamin interferometer, Rev. Sci. Instr., 77, 064903, https://doi.org/10.1063/1.2205623, 2006.

Song, Y., Pei, X., Liu, H., Zhou, J., and Wang, Z.: Characterization of tandem aerosol classifiers for selecting particles: implication for eliminating the multiple charging effect, Atmos. Meas. Tech., 15, 3513–3526, https://doi.org/10.5194/amt-15-3513-2022, 2022.

Szopa, S., Naik, V., Adhikary, B., Artaxoand, P., Berntsen, T., Collins, W., Fuzzi, S., Gallardo, L., Kiendler-Scharr, A., Klimont, Z., Liao, H., Unger, N., and Zanis, P.: Short-Lived Climate Forcers, Cambridge University Press, Cambridge, United Kingdom and New York, NY, USA, Chap. 6, 817–922, https://doi.org/10.1017/9781009157896.008, 2021.

Titosky, J., Momenimovahed, A., Corbin, J., Thomson, K., Smallwood, G., & Olfert, J. S.: Repeatability and intermediate precision of a mass concentration calibration system. Aerosol Science and Technology, 53(6), 701–711. https://doi.org/10.1080/02786826.2019.1592103, 2019.

https://doi.org/10.5194/egusphere-2026-1501
Preprint. Discussion started: 10 June 2026

Vandaele, A. C., Hermans, C., Fally, S., Carleer, M., Colin, R., Merienne, M. F., Jenouvrier, A., and Coquart, B.: High-resolution Fourier transform measurement of the NO2 visible and near infrared absorption cross sections: Temperature and pressure effects, J. Geophys. Res.-Atmos., 107, ACH 3-1–ACH 3-12, https://doi.org/10.1029/2001jd000971, 2002.

Vasilatou, K., Iida, K., Kazemimanesh, M., Olfert, J., Sakurai, H., Sipkens, T.A. and Smallwood, G.J.: Aerosol physical characterization: A review on the current state of aerosol documentary standards and calibration strategies, J. Aerosol Sci., 183, 106483- , https://doi.org/10.1016/j.jaerosci.2024.106483, 2025.

Virkkula, A., Mäkelä, T., Hillamo, R., Yli-Tuomi, T., Hirsikko, A., Hämeri, K., and Koponen, I. K.: A simple procedure for correcting loading effects of aethalometer data, J. Air Waste Manage., 57, 1214–1222, https://doi.org/10.3155/1047-3289.57.10.1214, 2007.

Weingartner, E., Saathoff, H., Schnaiter, M., Streit, N., Bitnar, B., and Baltensperger, U.: Absorption of light by soot particles: determination of the absorption coefficient by means of aethalometers, J. Aerosol Sci., 34, 1445–1463, https://doi.org/10.1016/S0021-8502(03)00359-8, 2003.

Wiedensohler, A., Wiesner, A., Weinhold, K., Birmili, W., Hermann, M., Merkel, M., Müller, T., Pfeifer, S., Schmidt, A., Tuch, T., Velarde, F., Quincey, P., Seeger, S., and Nowak, A.: Mobility particle size spectrometers: Calibration procedures and measurement uncertainties, Aerosol Sci. Technol., 52, 146–164, https://doi.org/10.1080/02786826.2017.1387229, 2018.

Yus-Díez, J., Bernardoni, V., Močnik, G., Alastuey, A., Ciniglia, D., Ivančič, M., Querol, X., Perez, N., Reche, C., Rigler, M., Vecchi, R., Valentini, S., and Pandolfi, M.: Determination of the multiple-scattering correction factor and its cross-sensitivity to scattering and wavelength dependence for different AE33 Aethalometer filter tapes: a multi-instrumental approach, Atmos. Meas. Tech., 14, 6335–6355, https://doi.org/10.5194/amt-14-6335-2021, 2021

Yus-Díez, J., Drinovec, L., Alados-Arboledas, L., Titos, G., Bazo, E., Casans, A., Patrón, D., Querol, X., Gonzalez-Romero, A., Perez García-Pando, C., and Močnik, G.: Characterization of filter photometer artifacts in soot and dust measurements – laboratory and ambient experiments using a traceably calibrated aerosol absorption reference, Atmos. Meas. Tech., 18, 3073–3093, https://doi.org/10.5194/amt-18-3073-2025, 2025.

Zanatta, M., Gysel, M., Bukowiecki, N., Muller, T., Weingartner, E., Areskoug, H., Fiebig, M., Yttri, K. E., Mihalopoulos, N., Kouvarakis, G., Beddows, D., Harrison, R. M., Cavalli, F., Putaud, J. P., Spindler, G., Wiedensohler, A., Alastuey, A., Pandolfi, M., Sellegri, K., Swietlicki, E., Jaffrezo, J. L., Baltensperger, U., and Laj, P.: A European aerosol phenomenology-5: Climatology of black carbon optical properties at 9 regional background sites across Europe, Atmos. Environ., 145, 346–364, https://doi.org/10.1016/j.atmosenv.2016.09.035, 2016.